Self-Inductance-Based Metal Object Detection With Mistuned Resonant Circuits and Nullifying Induced Voltage for Wireless EV Chargers

Seog Y. Jeong, *Student Member, IEEE*, Van X. Thai, *Student Member, IEEE*, Jun H. Park, *Student Member, IEEE*, and Chun T. Rim, *Senior Member, IEEE*

***Abstract*—In this paper, a metal object detection (MOD) system, a kind of foreign object detection (FOD), which is based on mistuned resonant circuits and utilizes the variation of self-inductance of a sensing pattern, is newly proposed for wireless electric vehicle (EV) chargers. The sensing pattern that consists of multiple loop coil sets is mounted on the transmitting (Tx) pad of an EV charger, where a loop coil set has two coils connected in series with the opposite polarity to cancel out the induced voltage generated by the Tx coil. Variation of self-inductance of the loop coil set is detected by a parallel-resonant circuit, driven by a current source and operating at near 1 MHz, in order to enhance the resolution of the proposed MOD system. To increase the detection sensitivity of the proposed MOD system, instead of an exact resonant frequency, a mistuned operating frequency near the –3 dB point is utilized for the parallel-resonant circuit. In this way, the proposed MOD system can detect very small metal objects regardless of their position and orientation on the Tx coil without any blind zone. Through simulations and experiments, it is found that the proposed MOD system detects not only horizontal but also standing upright metal objects. A prototype MOD system, operating at 85 kHz to satisfy the standard J2954, was fabricated to verify its feasibility. The results showed that output voltage change of the proposed MOD system becomes 22.7% for a piece of the aluminum foil of 3×3 cm^2 and 40.9% for 100 Korean Won coin.**

***Index Terms*—Blind zone, foreign object detection (FOD), metal object detection (MOD), mistuned resonance, wireless electric vehicle (EV) charger.**

I. Introduction

As INTEREST in and demand for electric vehicles (EVs) have increased in recent years, inductive power transfer

Manuscript received November 1, 2017; revised January 29, 2018; accepted March 4, 2018. Date of publication March 8, 2018; date of current version November 19, 2018. This work was supported by the Technology Innovation Program funded by the Ministry of Trade, Industry and Energy (MI, South Korea) (No. 20161210200740). Part of this original manuscript will be presented at the 2018 IEEE ECCE-ASIA. Recommended for publication by Associate Editor J. M. R. Davila. *(Corresponding author: Chun T. Rim.)*

S. Y. Jeong is with the Department of Nuclear and Quantum Engineering, Korea Advanced Institute of Science and Technology, Daejeon 305-755, South Korea. (e-mail:

In the meantime, MOD systems using an additional sensing pattern, where the loop coils are connected in the reverse direction to cancel out the induced voltage, have been introduced by KAIST and WiTricity [26]–[29]. The MOD system is able to detect small metal objects because the induced voltage of the sensing pattern, which is generated by the Tx coil, is theoretically set to zero, providing a simple, cheap, and suitable solution for high-power IPTSs. Although the method using the magnetic field generated by the Tx coil is effective, the sensing area is limited by the magnetic field generated by the Tx coil, which means there are some special areas called "blind zones" where metal objects cannot be detected or only can be partly detected [26]. In the case of multilayer construction of the sensing pattern, the majority of blind zones at the intersection of loop coils are resolved; however, blind zones may remain at points where the magnetic field generated by the Tx coil is weak or only the magnetic field component in the horizontal direction is present. Even if the temperature of the metal objects does not increase at these points, the MOD system must sense the metal objects because they are potential hazard.

In this paper, to resolve the problem of blind zones, the MOD system that utilizes the self-inductance change of a sensing pattern and a mistuned parallel-resonant circuit is newly proposed for wireless EV charger applications. The proposed MOD system can detect very small metal objects regardless of their position and orientation on the Tx pad with no blind zone. Additionally, in order to increase the detection sensitivity of the proposed MOD system, a mistuned operating frequency near –3 dB point is utilized instead of the exact resonant frequency of the parallel-resonant circuit. Theoretical analysis, simulations, and experiments are presented in the following sections to verify the proposed MOD system.

II. Principle of the Proposed System

The key idea of the proposed MOD system is to measure the impedance of the sensing pattern (simple loop coil shape; a detailed description will be introduced in the next section) considering the reflected impedance by metal objects, as shown in Fig. 1. The equivalent circuit model under the influence of metal objects around the sensing pattern based on mutual coupling modeling is shown in Fig. 2.

When metal objects are close to the sensing pattern, the equivalent impedance should be changed. The equivalent circuit model expressed by an inductor with a series resistor or a parallel resistor, respectively, can be expressed as

$$Z_{\mathrm{eq},s} = j\omega\alpha_s L_1 + \beta_s r_1 \tag{1a}$$

$$Z_{\mathrm{eq},p} = j\omega\alpha_p L_1 + \beta_p R_1 \tag{1b}$$

where L_1 and r_1 are the self-inductance and internal resistance of the sensing pattern without metal objects. R_1 is an equivalent parallel resistor of the sensing pattern without any metal objects. α, β_s, and β_p are defined as the variation ratio of L_1, r_1, and

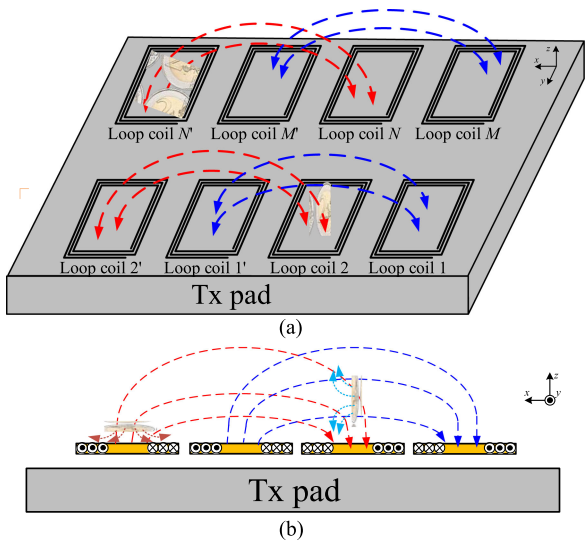

Fig. 1. Concept of the proposed MOD system, where metal objects are placed on the Tx pad. (a) Bird's eye view. (b) Front view, where loop coil *n* is connected in series with *n'*, $n \in \{1, 2, \ldots, M, N\}$.

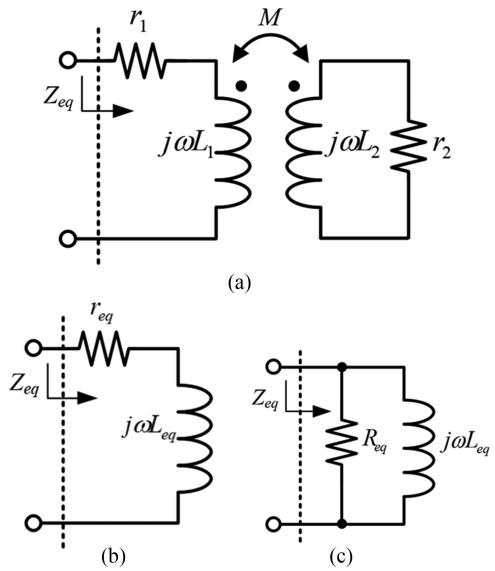

Fig. 2. (a) Equivalent circuit model of the sensing pattern under the influence of metal objects. (b) Simplified equivalent circuit model expressed by an inductor with a series resistor. (c) Simplified equivalent circuit expressed by an inductor with a parallel resistor.

R_1, as follows:

$$\alpha = \alpha_s \approx \alpha_p = 1 - \frac{L_2}{L_1} \cdot \frac{(\omega M)^2}{r_2^2 + \omega^2 L_2^2} \tag{2a}$$

$$\beta_s = 1 + \frac{r_2}{r_1} \cdot \frac{(\omega M)^2}{r_2^2 + \omega^2 L_2^2}, \quad \because \beta_p = \frac{\alpha^2}{\beta_s} \tag{2b}$$

where L_2 and r_2 are the equivalent inductance and resistance of the metal objects and M is the mutual inductance between the sensing pattern and the metal objects. Here, the subscripts "*s*," "*p*," "*w*," and "*wo*" denote "series," "parallel," "with metal objects," and "without metal objects," respectively. In general,

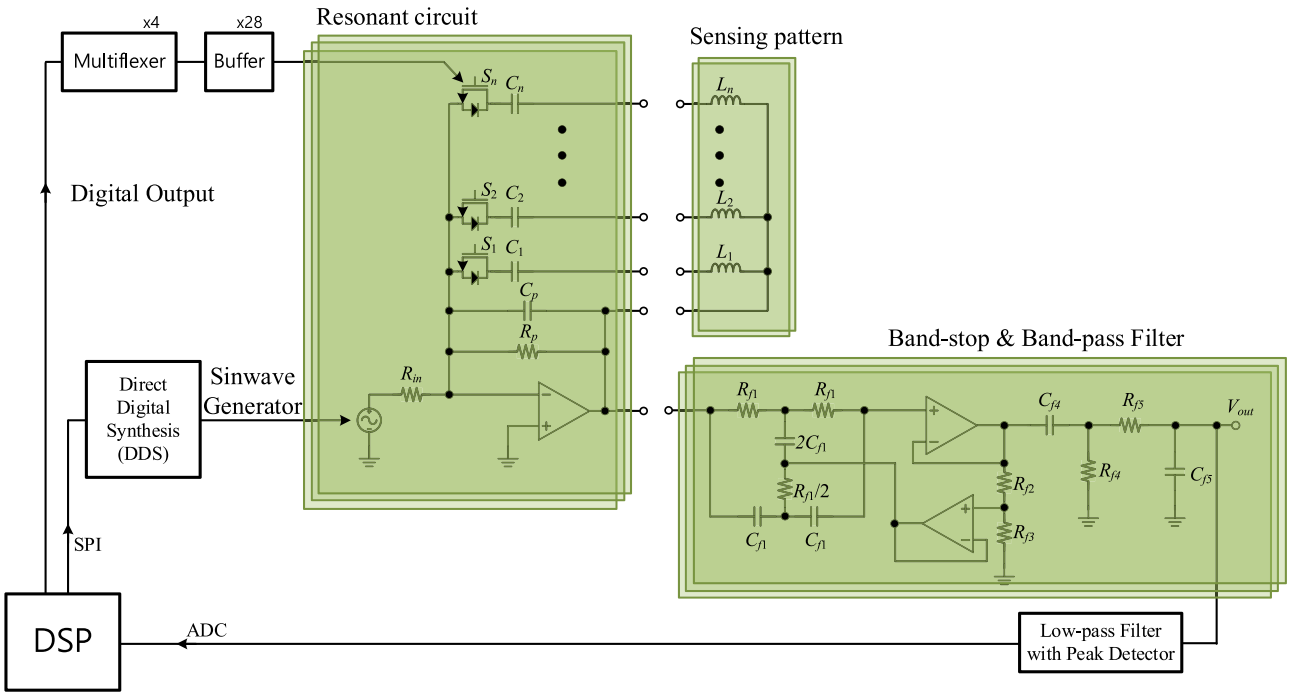

Fig. 3. Overall circuit configuration of the proposed MOD system.

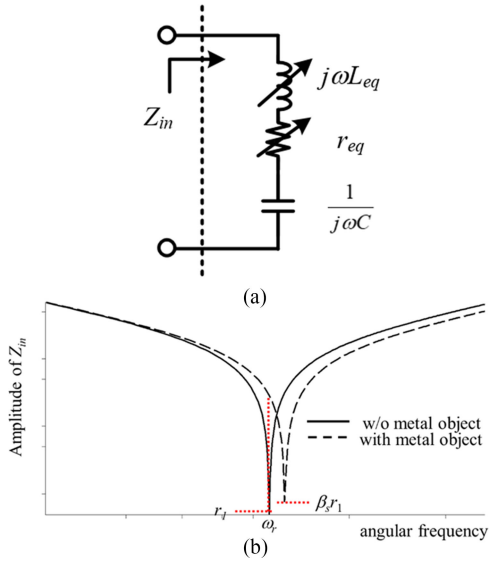

Fig. 4. (a) Equivalent circuit model for the series-resonant topology. (b) Its impedance characteristics.

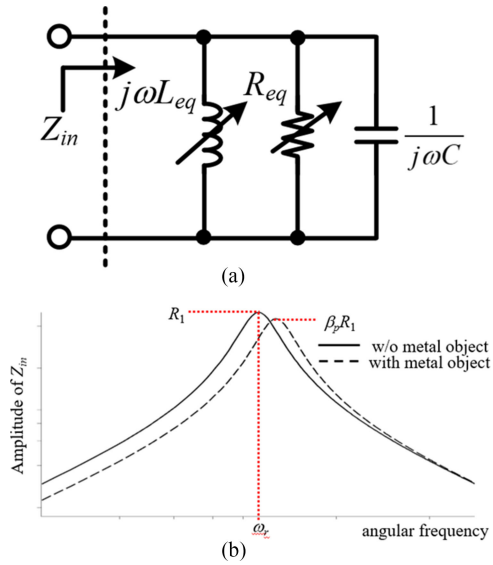

Fig. 5. (a) Equivalent circuit model for the parallel-resonant topology. (b) Its impedance characteristics.

the reactance of the metal objects ωL_2 is much bigger than r_2, being inversely proportional to the conductivity σ, and thereby the eddy current inside of the metal objects is out of phase with the current of the sensing pattern. From (1) and (2), the equivalent inductance L_{eq} always decreases by the influence of the metal objects, whereas the equivalent series resistance (ESR) r_{eq} always increases, resulting in an increase of the self-resonant frequency and conduction losses. It is not easy to apply the methods of the conventional metal detectors [41], [42] because a lot of high-frequency noise comes from the switching power system in the IPTS. Thereby, in case of wireless EV charger applications, the quality factor Q of the sensing pattern and the signal-to-noise ratio should be bigger than those of the conventional metal detector. In addition, the size of the sensing pattern is also limited depending on the metal objects since the detecting sensitivity is dramatically reduced when the metal objects are much smaller than the sensing pattern. The conventional sensing methods, such as the use of an ac signal without any modulation, make the system more complex and costly due to the noise and high operating frequency. Moreover,

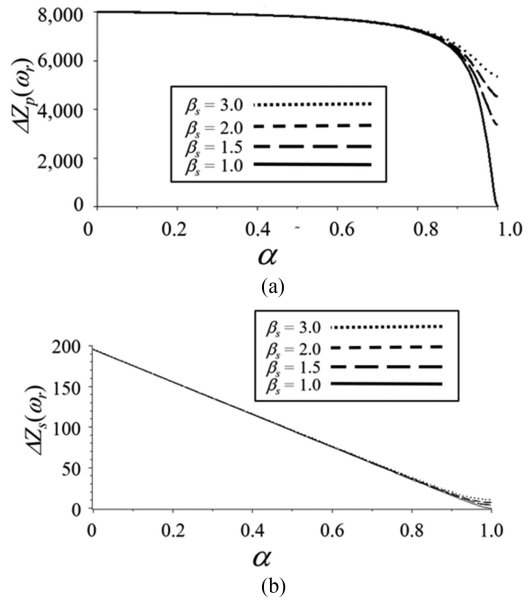

Fig. 6. Plots of impedance variation at resonant condition versus α and β_s with (a) parallel-resonant topology and (b) series-resonant topology.

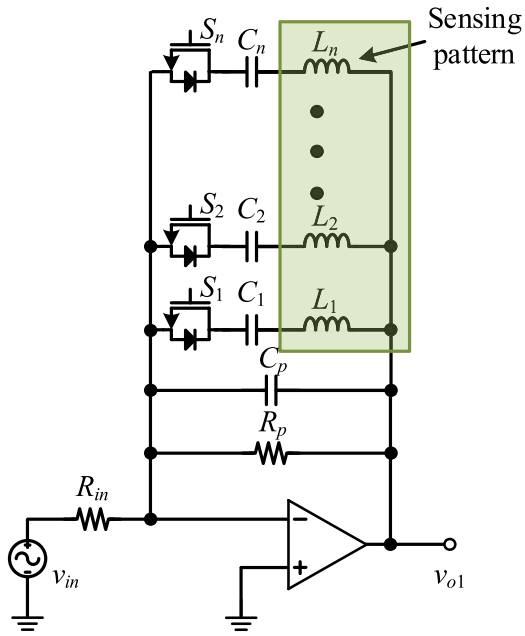

Fig. 7. Proposed parallel-resonant circuit with an inverting amplifier.

it is difficult to employ the MOD system directly in wireless EV charger applications because the impedance variation by a metal object may not be sufficient compared to the effects of noise.

As a remedy for this problem, a resonance topology is applied to the MOD system to amplify the impedance variation. The proposed MOD system consists of the sensing pattern, a parallel-resonant circuit, its driving circuit excited by a sine wave current source with angular frequency ω_s, and filters, as shown in Fig. 3. For a better understanding of the readers, the description of other parts is omitted.

A. Comparison Between Series/Parallel-Resonant Topologies

To amplify the impedance variation, two types of resonant circuits with an op-amp are compared: a series-resonant circuit and a parallel-resonant circuit. The series-resonant circuit and its impedance characteristics are shown in Fig. 4.

In the case of the series-resonant circuit without metal objects, the impedance of the equivalent circuit at angular resonant frequency ω_r should be designed as the minimum value (ideally zero for lossless component) where ω_r is defined as follows:

$$\omega_r = \frac{1}{\sqrt{L_{\text{eq}} C}}. \tag{3}$$

When a metal object is placed near the sensing pattern, L_{eq} and r_{eq} of the sensing pattern are changed to αL_1, and $\beta_s r_1$, respectively. Therefore, the impedance of the series-resonant circuit at ω_r increases, resulting in the deviation from the full resonance condition, as follows:

$$Z_{s,wo}(\omega_r) = r_1 \tag{4a}$$

$$Z_{s,w}(\omega_r) = -jQ_s(1-\alpha)r_1 + \beta_s r_1 \tag{4b}$$

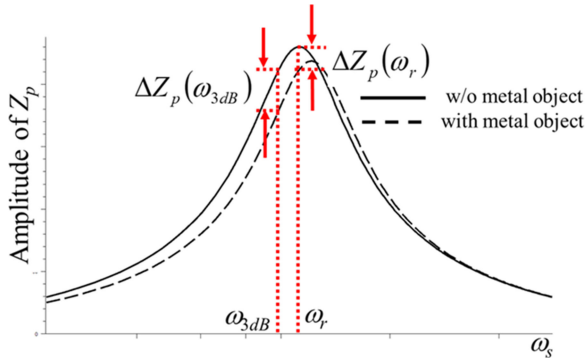

Fig. 8. Impedance characteristics for mistuned parallel-resonant at $\omega_{3\text{dB}}$.

where the quality factor Q_s of the series-resonant circuit without metal objects is defined as follows:

$$Q_s = \frac{1}{r_{\text{eq}}}\sqrt{\frac{L_{\text{eq}}}{C}}. \tag{5}$$

The impedance variation in the series-resonant circuit at the resonant condition $\Delta Z_s(\omega_r)$ can be obtained by subtracting the amplitude of (4a) from the amplitude of (4b), as follows:

$$\Delta Z_s(\omega_r) = r_1\left(\sqrt{{Q_s}^2(1-\alpha)^2 + {\beta_s}^2} - 1\right). \tag{6}$$

The parallel-resonant circuit and its impedance characteristics are also shown to find a better method, as shown in Fig. 5. In the case of the parallel-resonant circuit, its impedance is maximized (ideally infinite) when there is no metal object.

In contrast to the case of a series-resonant circuit, the impedance of a parallel-resonant circuit without the metal object at ω_r should be designed as the maximum value (ideally infinity for lossless components). When the metal objects are placed

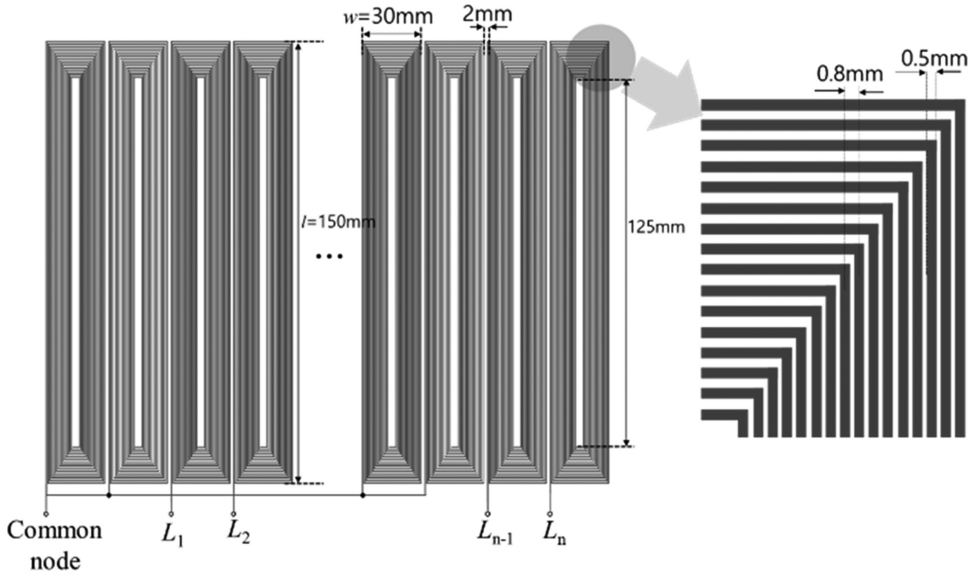

Fig. 9. Overall structure of the proposed sensing pattern.

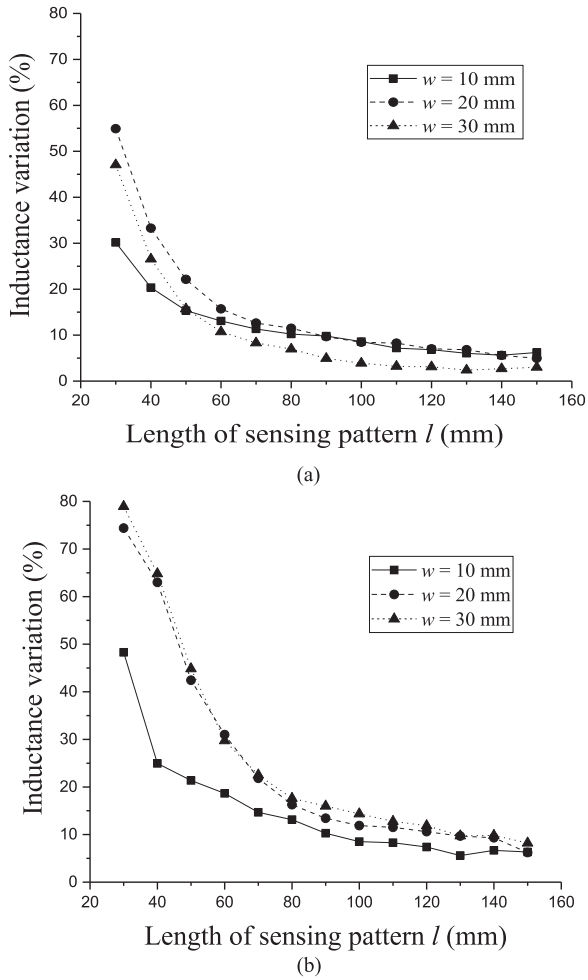

Fig. 10. Simulation results of self-inductance variation of the sensing pattern with respect to the length of sensing pattern l for an air-gap of 0.5 cm with a thin aluminum foil. (a) Size of the thin aluminum foil: $2 \times 2\,\mathrm{cm}^2$. (b) Size of the thin aluminum foil: $3 \times 3\,\mathrm{cm}^2$.

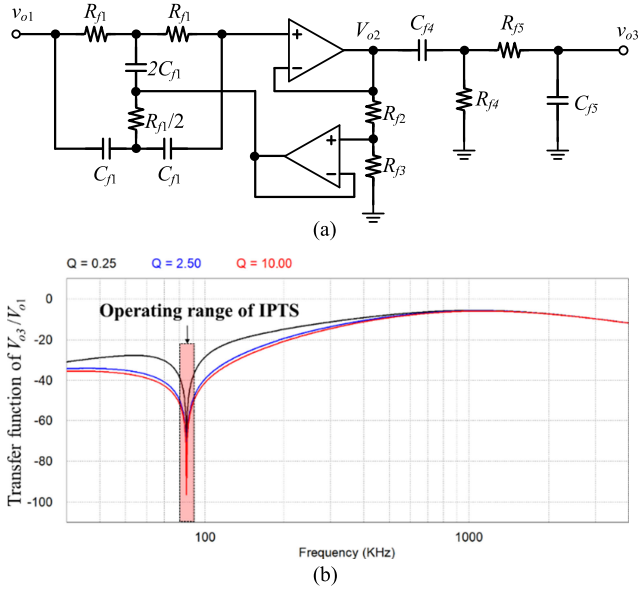

Fig. 11. (a) Circuit configuration of band-stop filter and band-pass filter. (b) Its transfer function.

near the sensing pattern, L_{eq} and r_{eq} of the sensing pattern are changed to αL_1 and $\beta_p R_1$, respectively. Here, the impedance of the parallel-resonant circuit at ω_r decreases, resulting in deviation from the full resonance condition, as follows:

$$Z_{p,wo}\left(\omega_r\right) = R_1 \tag{7a}$$

$$Z_{p,w}\left(\omega_r\right) = \frac{\beta_p R_1}{1 - jQ_p\beta_p\frac{1-\alpha}{\alpha}}. \tag{7b}$$

The quality factor Q_p of the parallel-resonant circuit without metal objects is defined as follows:

$$Q_p = R_{\mathrm{eq}}\sqrt{\frac{C}{L_{\mathrm{eq}}}}. \tag{8}$$

The impedance variation in the parallel-resonant circuit at a resonant condition $\Delta Z_p(\omega_r)$ can be also obtained by subtracting the amplitude of (7a) from the amplitude of (7b), as follows:

$$\Delta Z_p(\omega_r) = R_1\left(1-\beta_p/\sqrt{1+\left(Q_p\beta_p\frac{(1-\alpha)}{\alpha}\right)^2}\right) = r_1{Q_p}^2\left(1-1/\sqrt{\frac{{\beta_s}^2}{\alpha^4}+\left\{\frac{Q_s(1-\alpha)}{\alpha}\right\}^2}\right). \tag{9}$$

In order to compare two resonant topologies, the graphs for $\Delta Z_s(\omega_r)$ and $\Delta Z_p(\omega_r)$ versus α and β_s are drawn in Fig. 6. For both resonant topologies, impedance variation is more sensitive to α than β_s. $\Delta Z_p(\omega_r)$ is always bigger than $\Delta Z_s(\omega_r)$ for a high Q. In other words, the parallel-resonant circuit is more sensitive than the series-resonant circuit. The parallel-resonant circuit is also advantageous in that it is more insensitive to noise than the series-resonant circuit due to its high output voltage characteristic. Therefore, the parallel-resonant circuit is adopted in the proposed MOD system.

B. Mistuned Parallel-Resonant Circuit

The parallel-resonant circuit consists of an inverting amplifier, unidirectional MOSFETs S_n, blocking capacitors C_n, $n \in \{1, 2, \ldots, N\}$, a resonant capacitor C_p, and input side resistance R_{in}, as shown in Fig. 7.

Not only to increase the sensitivity of the proposed MOD system but also to simplify the circuit at the same time, unidirectional MOSFET switches control the parallel-resonant circuit time-divisionally. Common source terminals of all switches are connected to the virtual ground of the op-amp to simplify its driving circuit. A parallel feedback resistor R_p represents the equivalent resistance of the sensing pattern. If the ESR of the sensing pattern changes too much with respect to temperature variation, the MOD system can be stabilized by inserting an additional external resistor. However, it should be noted that if an excessively small resistor is inserted, Q of the parallel-resonance circuit decreases, leading to decreased sensitivity. The series capacitor C_n with a sufficiently large capacitance is connected in series with the switch to block the dc component. The parallel capacitor C_p forms a feedback loop to adjust ω_r of the parallel-resonant circuit. For easy control, ω_r should be kept at the same value for all sensing patterns, as follows:

$$\omega_r = \frac{1}{\sqrt{L_1(C_1||C_p)}} = \cdots = \frac{1}{\sqrt{L_n(C_n||C_p)}}. \tag{10}$$

The inverting amplifier boosts the out voltage (7b) times the input current. The op-amp with sufficient bandwidth should be selected since the closed-loop feedback gain is larger and the operating frequency is high. The transfer function of voltage gain is given as follows:

$$G_1(\omega) = \frac{V_{0,1}(\omega)}{V_{in}(\omega)} = \frac{1}{R_{in}}\cdot\frac{\beta_p R_1}{1+j\beta_p R_1(\omega C - 1/(\omega\alpha L_1))}. \tag{11}$$

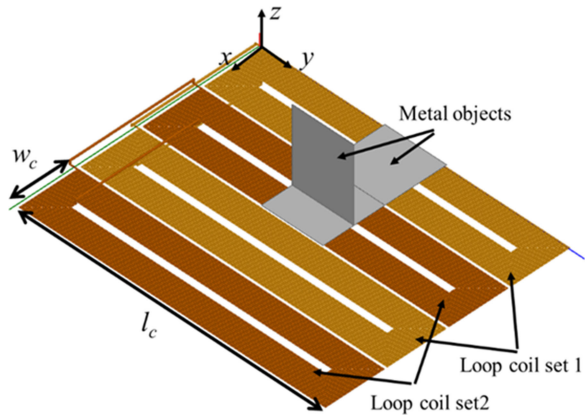

Fig. 12. Overall configuration of the FEM 3-D simulation for $N = 16$, $w_c = 3$ cm, and $l_c = 15$ cm.

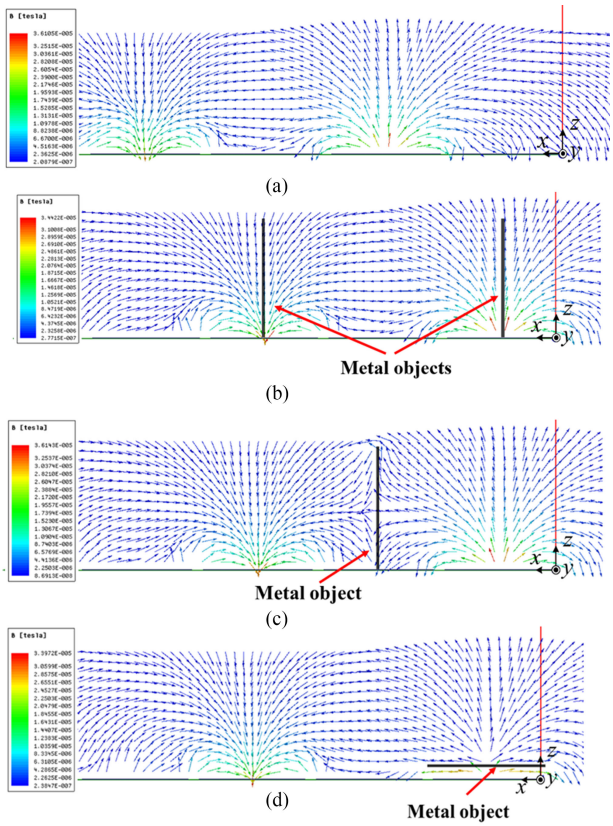

Fig. 13. FEM simulation results of magnetic field distribution of the sensing pattern. (a) When loop coil set 1 is excited without the metal objects. (b) When loop coil set 2 is excited where metal objects are placed perpendicularly to the loop coil set 2. (c) When loop coil set 2 is excited where the metal objects are placed perpendicularly to loop coil set 1. (d) When loop coil set 2 is excited where the metal objects are placed horizontally with loop coil set 2.

Slightly different from the previously mentioned, the operating angular frequency of the proposed MOD system is mistuned to -3 dB frequency $\omega_{3\mathrm{dB}}$ from ω_r since it is not easy to accurately track ω_r under the condition with a high Q, as shown in Fig. 8.

For example, if the operating frequency is incorrectly set as a higher value than ω_r, then when the metal objects are placed near the sensing pattern, there is a point at which the impedances are

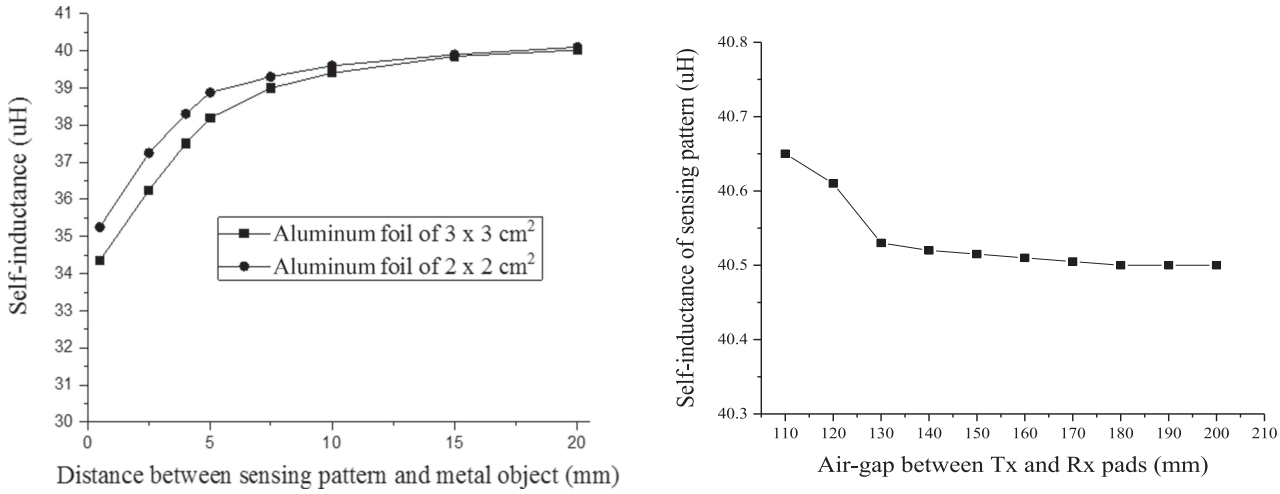

Fig. 14. Simulation results of self-inductance variation of the sensing pattern with respect to (a) distance between sensing pattern and metal object and (b) air-gap between Tx and Rx pads.

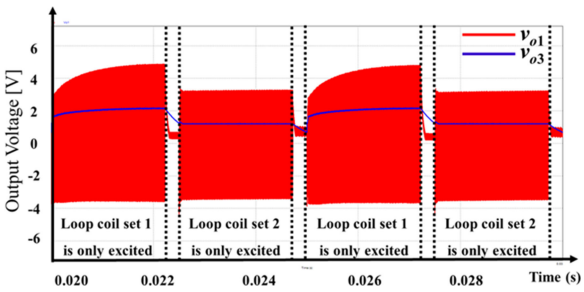

Fig. 15. Simulation results for operation verification of the proposed MOD system.

equal to each other. As a result, the MOD system cannot detect the metal objects due to the large amount of noise absorbed into the circuit. The second reason for employing the mistuned resonant condition is higher sensitivity. The variation of the impedance of $\omega_{3\mathrm{dB}}$, $\Delta Z_p(\omega)_{3\mathrm{dB}}$ in the area below ω_r is given as follows:

$$\begin{aligned}\Delta Z_p\left(\omega_{3\mathrm{dB}}\right) &\equiv \left|Z_{p\_wo}\left(\omega_{3\mathrm{dB}}\right)\right| - \left|Z_{p\_w}\left(\omega_{3\mathrm{dB}}\right)\right| \\ &\approx R_1\left(\frac{1}{\sqrt{2}} - \beta_p \Big/ \sqrt{1+\left\{Q_p\beta_p\frac{(1-\alpha)}{\alpha}\right\}^2}\right) \\ \because Z_{p\_w}\left(\omega_{3\mathrm{dB}}\right) &= \frac{\beta_p R_1}{1-j\beta_p\left\{1+\left(\frac{1-\alpha}{\alpha}\right)\left(\sqrt{{Q_p}^2+\frac{1}{4}}+\frac{1}{2}\right)\right\}}.\end{aligned} \tag{12}$$

From (13), $\Delta Z_p(\omega)_{3\mathrm{dB}}$ is always larger than $\Delta Z_p(\omega_r)$ regardless of α and β_p for high Q. Namely, the mistuned parallel-resonant circuit shows better performance

$$\Delta Z_p\left(\omega_{3\mathrm{dB}}\right) - \Delta Z_p\left(\omega_r\right) \approx R_1\left(\frac{1}{\sqrt{2}} - 1\right) > 0. \tag{13}$$

C. Designing Sensing Pattern

The sensing pattern, which consists of multiple loop coil sets in order to increase the sensitivity, is mounted on the Tx pad, where each loop coil set has two coils connected in series with the opposite polarity to cancel out the induced voltage generated by the Tx coil. Self-inductance change of the loop coil set is detected by the parallel-resonant circuit described in the previous section. Inductors of the sensing pattern, i.e., L_1, L_2, ..., and L_n, are connected to the common node, as shown in Fig. 9.

There are two major points to consider when designing the sensing pattern. First, the inductance variation and the number of sensing patterns should be designed in a tradeoff relationship. In order to confirm the tendency of inductance variation of the sensing pattern, simulation was performed while changing the size of the sensing pattern, as shown in Fig. 10.

As the size of the sensing pattern increases, its variation ratio decreases since the amount of the magnetic flux generated by the eddy current of the metal is relatively reduced compared to the amount of the magnetic flux generated by the sensing pattern. From the point where the length of the sensing pattern is less than about three times the width of the sensing pattern, the slope of the variation of inductance increases sharply.

The inductance variation by metal objects increases as the size of the sensing pattern becomes smaller; however, a number of sensing patterns are required to cover the entire area of the Tx pad. Moreover, the signal processing can be complex, not only because of long calculation time but also because of the response time by system dynamics. Hence, the optimum design is required to consider both the sensitivity of the sensing pattern and the number of sensing pattern; however, this lies beyond the scope of this paper. Second, the induced voltage on the sensing pattern generated by the switching power system in the IPTS should be taken into account. Although there are filters to eliminate the effect of the induced voltage in the proposed MOD system, the sensing pattern still should be carefully designed in

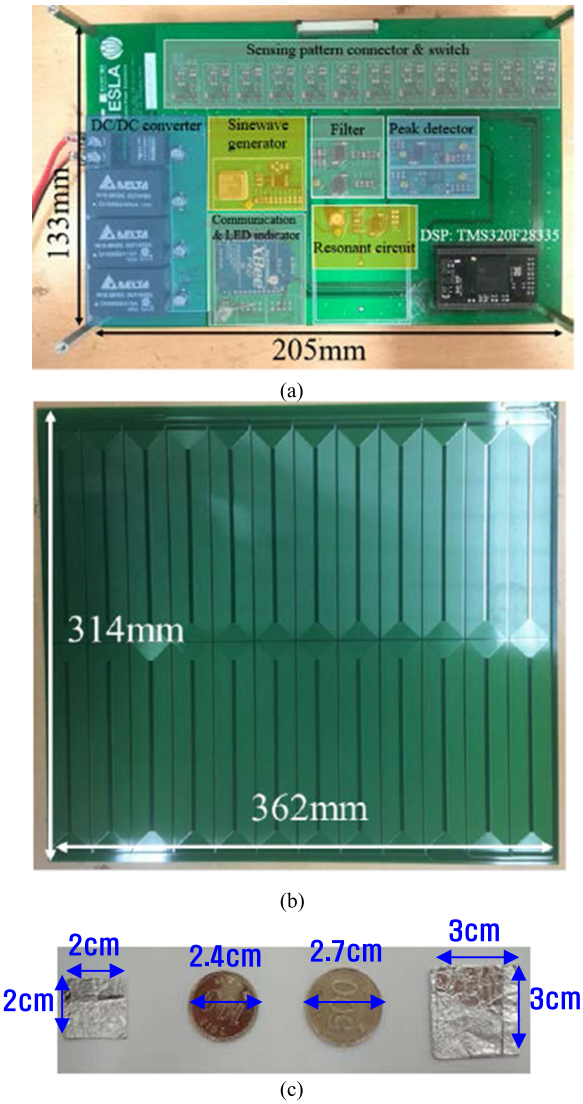

Fig. 16. Experiment condition. (a) Sensing circuit. (b) Sensing pattern. (c) Various metal objects.

order to cancel out the induced voltage. A simple method for this purpose is to adjust the number of turns of each loop coil sets so that the amount of linkage flux by the two loop coils is equal. To reduce the induced voltage, two loop coils can be connected in antiseries to cancel out the magnetic flux.

D. Filter Design and Frequency Selection

The filters can be roughly divided into two stages, as shown in Fig. 11(a). An active type of twin-T band-stop filter with the sum of two key properties, having the same magnitude and being out of phase with each other, is applied to the first stage to eliminate the induced voltage by the IPTS. The frequency response of the twin-T band-stop filter is shown in Fig. 11(b). It can be confirmed that the signal of 85 kHz by the switching power system in the IPTS is clearly attenuated by more than 60 dB keeping attenuation of the other signals to a minimum value. The resistances and capacitances are chosen according to the rules of the twin-T band-stop filter to filter out the 85 kHz signal [43].

The second stage is a band-pass filter to eliminate the effect by the dc offset voltage of the op-amp and high-frequency switching noise by the switching power system. If these signals are not attenuated sufficiently, then they may cause malfunction of the proposed MOD system. The center frequency of the band-pass filter is designed to match the operating frequency of the excited source, where the operation frequency of the proposed MOD system is chosen as 12 times the frequency of the switching power system in the IPTS, near 1 MHz. To pass only the signal of 1,020 kHz, a passive band-pass filter is simply applied, as shown in Fig. 11(a). The voltage gain of the filters is derived as follows:

$$G_2(\omega) \equiv \frac{V_{o3}(\omega)}{V_{o1}(\omega)} = \frac{1 - {a_1}^2\omega^2}{1 - {a_1}^2\omega^2 + j\omega a_1 a_2} \cdot \frac{a_3}{(a_3 + a_4) + j\left(\omega - \frac{a_3 a_4}{\omega}\right)}$$

$$\because a_1 = R_{f1}C_{f1} \quad a_2 = \frac{4R_{f2}}{R_{f2} + R_{f3}} \quad a_3 = R_{f4}C_{f4}$$

$$a_4 = R_{f5}C_{f5}. \tag{14}$$

III. Simulation Results

To identify the behavior of the magnetic field of the sensing pattern by the metal objects, FEM Maxwell simulations with only two loop coil sets are considered, as shown in Fig. 12. The magnetic flux is distorted by metal objects lying horizontally with the sensing pattern where the surface of the metal objects and the magnetic flux of the sensing pattern are not parallel, as shown in Fig. 13(c) and (d). In contrast, there is no distortion for metal objects lying vertically with the sensing pattern where the surface of the metal objects and the magnetic flux of the sensing pattern are parallel, as shown in Fig. 13(b), resulting in no eddy current inside the metal objects.

The simulation results for inductance variation depending on the height of the metal objects lying horizontally with the sensing pattern are shown in Fig. 14(a). The size of the sensing pattern is the same as the simulation condition, as shown in Fig. 12, where the Tx pad of $724 \times 628\,\text{mm}^2$ including ferrite core has been added under the sensing pattern. The inductance varies by 2.8% for an air-gap of 1 cm with a thin metal foil of $3 \times 3\,\text{cm}^2$. The self-inductance always decreases for air-gap decrease, whereas there is no change in the self-inductance when the metal is placed vertically with the sensing pattern. To cope with a blind zone by angle, another loop coil set lies alternately one by one. By measuring the self-inductance of the adjacent loop coil set shown in Fig. 13(c), it can be determined that there is no blind zone on the Tx pad over the entire area. Moreover, the effect by variation of air-gap between Tx and Rx pads is also important. If the inductance of the sensing pattern is varied by the Rx pad, it will be very difficult to match the mistuned resonant condition. Therefore, it is meaningful to check the variation of inductance by the Rx pad, the simulation results are shown in Fig. 14(b). The self-inductance checked that the air-gap between the Tx and Rx pads changes from 110 to 200 mm in 10 mm intervals, where air-gap between the Tx and Rx pads

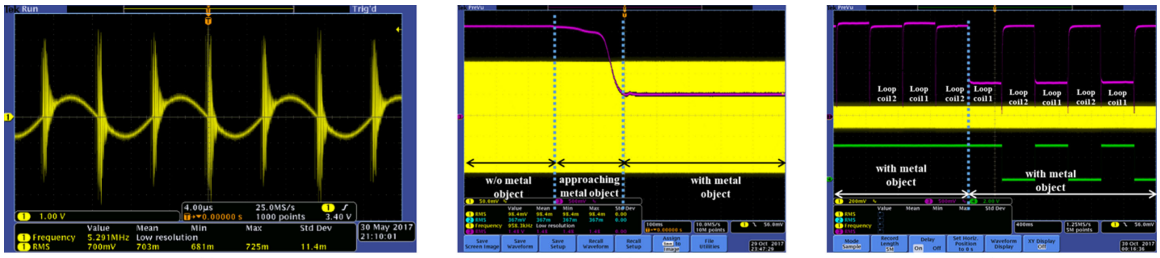

(a) (b) (c)

Fig. 17. (a) $v_{o1}(t)$ wave form considering the high-frequency noise without excited current. (b) Output voltage $v_{o3}(t)$ when $3 \times 3\,\text{cm}^2$ piece of the aluminum foil is put at the center of loop coil set 1. (c) Multichannel operation of (b).

from 130 to 200 mm is generally used for wireless EV charger applications. Through the simulation results, it was confirmed that the self-inductance of the sensing pattern is not affected by the variation of air-gap or misalignment in air-gap over 130 mm because the distance between the sensing pattern and the Rx pad is much larger than the width of the sensing pattern. In other words, it does not require initial calibration according to the presence of EVs.

To verify the operation of the proposed MOD system, only two sensing coil are simulated by the PSIM 9.1.1 circuit simulation tool where all circuit parameters including filters and peak detector are designed based on the results in the previous chapter, as shown in Fig. 15. When the self-inductance is changed from 40.05 to 38.20 μH (about variation of 5%), the output voltage decreases from 4.7 to 3.2 V, falling to 68% compared to the case without the metal objects, with a dynamic response of 10 ms.

IV. Experimental Results

The experiment was set up, as shown in Fig. 16. The Tx pad and fabricated sensing pattern for the experiments were 724×628 and $314 \times 612\,\text{mm}^2$ in size, respectively. The sensing pattern was fabricated to detect only one-quarter of the size of the Tx pad for laboratory verification since the magnetic field distribution on the Tx pad is symmetrical about front and rear and left and right. The size of the loop coil was determined to $3 \times 15\,\text{cm}^2$ considering detection of metal objects with a size of $3 \times 3\,\text{cm}^2$ and the number of loop coil sets being 50 or less.

The open voltage of the sensing pattern was measured when Tx current of 20 A_{rms}, satisfying 6.6 kW power transfer, was applied to monitor how much noise is coming in. As shown in Fig. 17(a), 0.7 V_{rms} with the fundamental frequency of 85 kHz and 6 V_{pp} high-frequency switching noise were induced. When a $3 \times 3\,\text{cm}^2$ piece of the aluminum foil is put at the center of the loop coil set 1, the output voltage decreased from 2.2 to 0.5 V, as shown in Fig. 17(b) and (c), where the 85 kHz noise only remains by less than 40 mV, in terms of signal processing, it can be rendered negligible by using various methods such as a filtering algorithm.

Experiments results for various metal objects and position are shown in Table I. The voltage of the proposed MOD system decreased by more than 30% for four metal specimens at air-gap of 5 mm. The possibility of the proposed MOD system for wireless EV charger applications, thus, has been verified.

TABLE I
Output Voltage Variation for Various Specimens

Metal types	Relative permeability	Conductivity	Output voltage variation
100 KRW coin (Diameter: 24 mm)	75.0	4.82×10^7	0.9 V
500 KRW coin (Diameter: 26.5 mm)	75.0	4.82×10^7	1.2 V
Aluminum foil of $2 \times 2\,\text{cm}^2$	1.0	3.54×10^7	0.7 V
Aluminum foil of $3 \times 3\,\text{cm}^2$	1.0	3.54×10^7	1.7 V

V. Conclusion

In this paper, a new MOD system that can detect the entire area on the Tx pad of wireless EV charger applications without any blind zone has been proposed. A parallel-resonant circuit with mistuned operating frequency near the –3 dB point has been used to increase the detection sensitivity of metal objects. In this way, it can detect very small metal objects regardless of their position and orientation on the Tx pad. It has also been confirmed that multiple loop coil sets can be operated by only one signal processing circuit with electronic switches. A prototype of the MOD system on the Tx pad, operating at 85 kHz to satisfy the standard J2954, was fabricated, and it showed that the output voltage was reduced by 22.7% for a piece of the aluminum foil of $3 \times 3\,\text{cm}^2$ and 40.9% for 100 Korean Won coin.

References

[1] J. Huh, S. W. Lee, W. Y. Lee, G. H. Cho, and C. T. Rim, "Narrow-width inductive power transfer system for online electrical vehicles," *IEEE Trans. Power Electron.*, vol. 26, no. 12, pp. 3666–3679, Dec. 2011.

[2] W. Y. Lee *et al.*, "Finite-width magnetic mirror models of mono and dual coils for wireless electric vehicles," *IEEE Trans. Power Electron.*, vol. 28, no. 3, pp. 1413–1428, Mar. 2013.

[3] S. Choi, J. Huh, S. Lee, and C. T. Rim, "New cross-segmented power supply rails for roadway powered electric vehicles," *IEEE Trans. Power Electron.*, vol. 28, no. 12, pp. 5832–5841, Dec. 2013.

[4] S. Lee, B. Choi, and C. T. Rim, "Dynamics characterization of the inductive power transfer system for on-line electric vehicles by Laplace phasor transform," *IEEE Trans. Power Electron.*, vol. 28, no. 12, pp. 5902–5909, Dec. 2013.

[5] S. Y. Choi, B. W. Gu, S. W. Lee, W. Y. Lee, J. Huh, and C. T. Rim, "Generalized active EMF cancel methods for wireless electric vehicles," *IEEE Trans. Power Electron.*, vol. 29, no. 11, pp. 5770–5783, Nov. 2014.

[6] S. Y. Choi, B. W. Gu, J. Huh, W. Y. Lee, J. G. Cho, and C. T. Rim, "Asymmetric coil sets for wireless stationary EV chargers with large lateral tolerance by dominant field analysis," *IEEE Trans. Power Electron.*, vol. 29, no. 12, pp. 6406–6420, Dec. 2014.

[7] S. Y. Choi, B. W. Gu, S. Y. Jeong, and C. T. Rim, "Advances in wireless power transfer systems for roadway powered electric vehicles," *IEEE J. Emerging Sel. Topics Power Electron.*, vol. 3, no. 1, pp. 18–36, Mar. 2015.

[8] S. Y. Choi, S. Y. Jeong, E. S. Lee, B. W. Gu, S. W. Lee, and C. T. Rim, "Generalized models on self-decoupled dual pick-up coils for a large lateral tolerance," *IEEE Trans. Power Electron.*, vol. 30, no. 11, pp. 6434–6445, Nov. 2015.

[9] S. Y. Choi, B. W. Gu, S. Y. Jeong, G. C. Lim, and C. T. Rim, "Ultra slim s-type power supply rails for roadway powered electric vehicles," *IEEE Trans. Power Electron.*, vol. 30, no. 11, pp. 6456–6468, Nov. 2015.

[10] C. Park, S. Lee, S. Y. Jeong, G. H. Cho, and C. T. Rim, "Uniform power I-type inductive power transfer system with DQ-power supply rails for on-line electric vehicles," *IEEE Trans. Power Electron.*, vol. 30, no. 11, pp. 6446–6455, Nov. 2015.

[11] C. Mi, G. Buja, S. Y. Choi, and C. T. Rim, "Modern advances in wireless power transfer systems for roadway powered electric vehicles," *IEEE Trans. Ind. Electron.*, vol. 63, no. 10, pp. 6533–6545, Oct. 2016.

[12] S. Y. Jeong *et al.*, "DQ-quadrature coil sets with large tolerance for wireless stationary EV chargers," in *Proc. IEEE PELS Workshop Emerging Technol., Wireless Power Transf.*, Jun. 2015, pp. 1–6.

[13] S. Li and C. C. Mi, "Wireless power transfer for electric vehicle applications," *IEEE J. Emerging Sel. Topics Power Electron.*, vol. 3, no. 1, pp. 4–17, Mar. 2015.

[14] A. Tejeda, C. Carretero, J. T. Boys, and G. A. Covic, "Ferrite-less circular pad with controlled flux cancelation for EV wireless charging," *IEEE Trans. Power Electron.*, vol. 32, no. 11, pp. 8349–8359, Nov. 2017.

[15] H. Zeng, S. Yang, and F. Z. Peng, "Design consideration and comparison of wireless power transfer via harmonic current for PHEV and EV wireless charging," *IEEE Trans. Power Electron.*, vol. 32, no. 8, pp. 5943–5952, Aug. 2017.

[16] T. Kan, T.-D. Nguyen, J. C. White, R. K. Malhan, and C. C. Mi, "A new integration method for an electric vehicle wireless charging system using LCC compensation topology: analysis and design," *IEEE Trans. Power Electron.*, vol. 32, no. 2, pp. 1638–1650, Feb. 2017.

[17] S. C. Moon and G.-W. Moon, "Wireless power transfer system with an asymmetric four-coil resonator for electric vehicle battery chargers," *IEEE Trans. Power Electron.*, vol. 31, no. 10, pp. 6844–6854, Oct. 2016.

[18] W. Zhang, J. C. White, A. M. Abraham, and C. C. Mi, "Loosely coupled transformer structure and interoperability study for EV wireless charging systems," *IEEE Trans. Power Electron.*, vol. 30, no. 11, pp. 6356–6367, Nov. 2015.

[19] B. Esteban, M. Sid-Ahmed, and N. C. Kar, "A comparative study of power supply architectures in wireless EV charging systems," *IEEE Trans. Power Electron.*, vol. 30, no. 11, pp. 6408–6422, Nov. 2015.

[20] S. Y. Jeong, H. G. Kwak, G. C. Jang, and C. T. Rim, "Living object detection system based on comb pattern capacitive sensor for wireless EV chargers," in *Proc. IEEE 2nd Annu. Southern Power Electron. Conf.*, Dec. 2016, pp. 1–6.

[21] Y. H. Sohn, B. H. Choi, E. S. Lee, and C. T. Rim, "Comparisons of magnetic field shaping methods for ubiquitous wireless power transfer," in *Proc. IEEE PELS Workshop Emerging Technol., Wireless Power Transf.*, Jun. 2015, pp. 1–6.

[22] S. Y. Jeong, E. S. Lee, C. B. Park, and C. T. Rim, "Influences of spurious conductors on long distance inductive power transfer systems," in *Proc. IEEE VTC Workshop Emerging Technol., Wireless Power*, May 2014, pp. 16–20.

[23] S. Fukuda, H. Nakano, Y. Murayama, T. Murakami, O. Kozakai, and K. Fujimaki, "A novel metal detector using the quality factor of the secondary coil for wireless power transfer systems," in *Proc. IEEE Int. Microw. Workshop Ser. Innov. Wireless Power Transm., Technol., Syst., Appl.*, May 2012, pp. 241–244.

[24] Z. N. Low, J. J. Casanova, P. H. Maier, J. A. Taylor, R. A. Chinga, and J. Lin, "Method of load/fault detection for loosely coupled planar wireless power transfer system with power delivery tracking," *IEEE Trans. Ind. Electron.*, vol. 57, no. 10, pp. 1478–1486, Apr. 2010.

[25] N. Kuyvenhoven, C. Dean, J. Melton, J. Schwannecke, and A. E. Umenei, "Development of a foreign object detection and analysis method for wireless power systems," in *Proc. IEEE Symp. Product Compliance Eng.*, Oct. 2011, pp. 1–6.

[26] S. Y. Jeong, H. G. Kwak, G. C. Jang, S. Y. Choi, and C. T. Rim, "Dual-purpose non-overlapping coil sets as metal object and vehicle position detections for wireless stationary EV chargers," *IEEE Trans. Power Electron.*, Oct. 2017, doi: 10.1109/TPEL.2017.2765521.

[27] G. C. Jang, S. Y. Jeong, H. G. Kwak, and C. T. Rim, "Metal object detection circuit with non-overlapped coils for wireless EV chargers," in *Proc. IEEE 2nd Annu. Southern Power Electron. Conf.*, Dec. 2016, pp. 1–6.

[28] S. Verghese, M. P. Kesler, K. L. Hall, and H. T. Lou, "Foreign object detection in wireless energy transfer systems," U.S. Patent 20 130 069 441 A1, Mar. 21, 2013.

[29] B. Zhou, Z. Z. Liu, H. X. Chen, H. Zeng, and T. Hei, "A new metal detection method based on balanced coil for mobile phone wireless charging system," in *Proc. Int. Conf. New Energy Future Energy Syst.*, Aug. 2016, pp. 1–9.

[30] G. Ombach, "Design considerations for wireless charging system for electric and plug-in hybrid vehicles," in *Proc. IEEE Hybrid Electr. Veh. Conf.*, Nov. 2013, pp. 1–4.

[31] G. Ombach, "Design and safety considerations of interoperable wireless charging system for automotive," in *Proc. 9th Int. Conf. Ecol. Veh. Renew. Energies*, Mar. 2014, pp. 1–4.

[32] J.-W. Jeong, S.-H. Ryu, B.-K. Lee, and H.-J. Kim, "Tech tree study on foreign object detection technology in wireless charging system for electric vehicles," in *Proc. IEEE Int. Telecommun. Energy Conf.*, Oct. 2015, pp. 1–4.

[33] X. Zhang, Y. Jin, Q. Yang, Z. Yuan, H. Meng, and Z. Wang, "Detection of metal obstacles in wireless charging system of electric vehicle," in *Proc. IEEE PELS Workshop Emerging Technol., Wireless Power Transf.*, May 2017, pp. 89–92.

[34] A. Razavi, R. Maaskant, J. Yang, and M. Viberg, "Optimal aperture distribution for near-field detection of foreign objects in lossy media," in *Proc. IEEE-APS Topical Conf. Antennas Propag. Wireless Commun.*, Aug. 2014, pp. 659–662.

[35] H. Kudo, K. Ogawa, N. Oodachi, N. Deguchi, and H. Shoki, "Detection of a metal obstacle in wireless power transfer via magnetic resonance," in *Proc. IEEE 33rd Int. Telecommun. Energy Conf.*, Oct. 2011, pp. 1–6.

[36] S. Y. Jeong, V. X. Thai, J. H. Park, H. G. Kwak, and C. T. Rim, "Self-inductance based metal object detection with mistuned resonant circuits and nullifying induced voltage for wireless EV chargers," in *Proc. IEEE Energy Convers. Congr. Expo. Asia*, to be published.

[37] X. Qunyu, N. Huansheng, and C. Weishi, "Video-based foreign object debris detection," in *Proc. IEEE Int. Workshop Imag. Syst. Techn.*, May 2009, pp. 119–122.

[38] S. Futatsumori, K. Morioka, A. Kohmura, and N. Yonemoto, "Design and measurement of W-band offset stepped parabolic reflector antennas for airport surface foreign object debris detection radar systems," in *Proc. IEEE Int. Workshop Antenna Technol.*, Mar. 2014, pp. 51–52.

[39] T. Kato, Y. Ninomiya, and I. Masaki, "An obstacle detection method by fusion of radar and motion stereo," *IEEE Trans. Intell. Trans. Syst.*, vol. 3, no. 3, pp. 182–188, Sep. 2002.

[40] A. Kohmura, S. Futatsumori, N. Yonemoto, and K. Okada, "Fiber connected millimeter-wave radar for FOD detection on runway," in *Proc. IEEE Eur. Radar Conf.*, Oct. 2013, pp. 41–44.

[41] H. Huang and I. J. Won, "Automated identification of buried landmines using normalized electromagnetic induction spectroscopy," *IEEE Trans. Geosci. Remote Sens.*, vol. 41, no. 3, pp. 640–651, Mar. 2003.

[42] S. Yamazaki, H. Nakane, and A. Tanaka, "Basic analysis of a metal detector," *IEEE Trans. Instrum. Meas.*, vol. 51, no. 4, pp. 810–814, Aug. 2002.

[43] M. Biey, "Design of twin-T single amplifier building block with prescribed values of capacitors and minimum gain-sensitivity product," *IEE Electron. Lett.*, vol. 17, no. 7, pp. 249–250, Apr. 1891.

Seog Y. Jeong (S'14) received the B.S. degree in electrical engineering from Kyungpook National University, Daegu, South Korea, in 2012, and the M.S. and Ph.D. degrees in nuclear quantum engineering from the Korea Advanced Institute of Science and Technology, Daejeon, South Korea, in 2015 and 2018, respectively.

He is currently a Postdoctoral Researcher with the Gwangju Institute of Science and Technology, Gwangju, South Korea. His current research interests include roadway-powered electric vehicle and wireless power transfers.

Van X. Thai (S'15) received the B.S. degree in electrical engineering from the Hanoi University of Science and Technology, Hanoi, Vietnam, in 2010, and the M.S. degree in nuclear and quantum engineering from the Korea Advanced Institute of Science and Technology, Daejeon, South Korea, in 2013. He is currently working toward the Ph.D. degree in electrical engineering at the Gwangju Institute of Science and Technology, Gwangju, South Korea.

His research interests include power electronics, power converters, and wireless power transfer.

Jun H. Park (S'17) received the B.S. degree in electronic engineering from Hanyang University, Seoul, South Korea, in 2017. He is currently working toward the M.S. degree at the Gwangju Institute of Science and Technology, Gwangju, South Korea.

His current research interests include roadway-powered electric vehicles and wireless power transfer.

Chun T. Rim (M'90–SM'11) received the B.S. degree (Hons.) from the Kumoh Institute of Technology, Gumi, South Korea, in 1985, and the M.S. and Ph.D. degrees from the Korea Advanced Institute of Science and Technology (KAIST), Daejeon, South Korea, in 1987 and 1990, respectively, all in electrical engineering.

In 2007–2016, he was an Associate Professor with the KAIST, and currently he is a Full Professor with the Gwangju Institute of Science and Technology, Gwangju, South Korea. He has authored or coauthored 160 technical papers, written 14 books, and holds 150 patents (awarded and pending).

Dr. Rim was a recipient of numerous awards, including the Best Paper Award of the IEEE TRANSACTIONS ON POWER ELECTRONICS (IEEE TPEL) in 2015 and the IEEE JOURNAL OF EMERGING AND SELECTED TOPICS IN POWER ELECTRONICS (IEEE J-ESTPE) in 2016 both in wireless power transfer (WPT). He is currently an Associate Editor for the IEEE TPEL and the IEEE J-ESTPE, a Guest Editor of the Special Issue on WPT for the IEEE TPEL, the IEEE TRANSACTIONS ON INDUSTRIAL ELECTRONICS, and the IEEE J-ESTPE, and the General Chair of the 2015 and 2016 IEEE Workshop on Wireless Power.